European Journal of Pharmacology 935 (2022) 175321

Contents lists available at ScienceDirect

European Journal of Pharmacology

journal homepage: www.elsevier.com/locate/ejphar

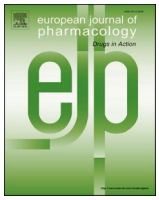

Pharmacologic characterization of TBP1901, a prodrug form of aglycone curcumin, and CRISPR-Cas9 screen for therapeutic targets of aglycone curcumin

Tomoyuki Abe [a], Yoshihito Horisawa [b], Osamu Kikuchi [c], Hitomi Ozawa-Umeta [a], Atsuhiro Kishimoto [a], Yasuhiro Katsuura [a], Atsushi Imaizumi [a], Tadashi Hashimoto [a], Kotaro Shirakawa [b], Akifumi Takaori-Kondo [b], Kosuke Yusa [d], Tadashi Asakura [e], Hideaki Kakeya [f,**], Masashi Kanai [c,*]

[a] Therabiopharma Inc., Kanagawa, Japan
[b] Department of Hematology and Oncology, Graduate School of Medicine, Kyoto University, Kyoto, Japan
[c] Department of Therapeutic Oncology, Graduate School of Medicine, Kyoto University, Kyoto, Japan
[d] Stem Cell Genetics, Institute for Frontier Life and Medical Sciences, Kyoto University, Kyoto, Japan
[e] Radioisotope Research Facilities, Jikei University School of Medicine, Tokyo, Japan
[f] Department of System Chemotherapy and Molecular Sciences, Division of Medicinal Frontier Sciences, Graduate School of Pharmaceutical Sciences, Kyoto University, Kyoto, Japan

ARTICLE INFO

Keywords:
β-Glucuronidase
Prodrug
NF-κB
Reactive oxgen species
Multi-target

ABSTRACT

Curcumin (aglycone curcumin) has antitumor properties in a variety of malignancies via the alteration of multiple cancer-related biological pathways; however, its clinical application has been hampered due to its poor bioavailability. To overcome this limitation, we have developed a synthesized curcumin β-D-glucuronide sodium salt (TBP1901), a prodrug form of aglycone curcumin. In this study, we aimed to clarify the pharmacologic characteristics of TBP1901. In β-glucuronidase (GUSB)-proficient mice, both curcumin β-D-glucuronide and its active metabolite, aglycone curcumin, were detected in the blood after TBP1901 injection, whereas only curcumin β-D-glucuronide was detected in GUSB-impaired mice, suggesting that GUSB plays a pivotal role in the conversion of TBP1901 into aglycone curcumin in vivo. TBP1901 itself had minimal antitumor effects in vitro, whereas it demonstrated significant antitumor effects in vivo. Genome-wide clustered regularly interspaced short palindromic repeats (CRISPR)-Cas9 screen disclosed the genes associated with NF-κB signaling pathway and mitochondria were among the highest hit. In vitro, aglycone curcumin inhibited NF-kappa B signaling pathways whereas it caused production of reactive oxygen species (ROS). ROS scavenger, *N*-acetyl-L-cysteine, partially reversed antitumor effects of aglycone curcumin. In summary, TBP1901 can exert antitumor effects as a prodrug of aglycone curcumin through GUSB-dependent activation.

1. Introduction

Curcumin (aglycone curcumin) is a natural polyphenol molecule derived from turmeric (*Curcumin longa*) that has shown antitumor effects in a number of preclinical models by modulating multiple biological targets including NF-κB, proteasome, or reactive oxygen species (ROS) (Banerjee et al., 2019; Bharti et al., 2003; Kunnumakkara et al., 2007; Larasati et al., 2018; Milacic et al., 2008; Mizumoto et al., 2019). Several clinical studies have reported the anecdotal efficacy of oral aglycone curcumin in patients with cancer (Dhillon et al., 2008; Kanai et al., 2011; Ramakrishna et al., 2020; Zaidi et al., 2017); however, its clinical application has been hampered due to its poor bioavailability and low stability. To overcome these problems, novel formulations with improved bioavailability have been developed and some have already

* Corresponding author. Therapeutic Oncology, Graduate School of Medicine, Kyoto University, 54 Shogoin-Kawahara-cho, Sakyo-ku, Kyoto, 606-8507, Japan.
** Corresponding author. Department of System Chemotherapy and Molecular Sciences, Division of Medicinal Frontier Sciences, Graduate School of Pharmaceutical Sciences, Kyoto University, 46-29 Shimo-Adachi-cho, Yoshida, Sakyo-ku, Kyoto, 606-8501, Japan.
E-mail addresses: scseigyo-hisyo@pharm.kyoto-u.ac.jp (H. Kakeya), kanai@kuhp.kyoto-u.ac.jp (M. Kanai).

https://doi.org/10.1016/j.ejphar.2022.175321
Received 25 April 2022; Received in revised form 4 October 2022; Accepted 5 October 2022
Available online 10 October 2022

been tested in clinical trials (Antony et al., 2008; Asher et al., 2017; Greil et al., 2018; Jager et al., 2014; Kanai et al., 2012, 2013; Marczylo et al., 2007; Stohs et al., 2020). Greil et al. developed an injectable form of aglycone curcumin using a liposomal delivery system and its safety was evaluated in heavily pretreated patients with cancer (Greil et al., 2018). However, due to hemolysis toxicity linked to liposomes, the mean maximum drug concentration (C_{max}) of aglycone curcumin was limited to 3.9 μM at maximum tolerated dose (MTD) of 300 mg/m^2. This C_{max} was higher than the C_{max} values reported in any orally administered formulations (Antony et al., 2008; Asher et al., 2017; Jager et al., 2014; Kanai et al., 2012, 2013; Marczylo et al., 2007); however, it appeared to be insufficient for deriving the maximum antitumor effects of aglycone curcumin. Recently, we have developed a synthetic curcumin β-D-glucuronide (CMG), which is a water-soluble molecule and can be administered intravenously. In vivo, CMG is partly converted into aglycone curcumin and can achieve more than 1000 times higher plasma aglycone curcumin levels compared with oral aglycone curcumin (Ozawa et al., 2017). Furthermore, CMG demonstrated superior antitumor effects on colon cancer xenograft model with less toxicity (Ozawa-Umeta et al., 2020). However, the exact mechanisms of CMG conversion into aglycone curcumin are still unknown. Furthermore, since aglycone curcumin can influence multiple cancer-related biological pathways (Prasad et al., 2014), it has been difficult to prioritize the therapeutic targets for its antitumor effects. Recent advances of clustered regularly interspaced short palindromic repeats (CRISPR) technology have made it possible to screen essential therapeutic targets of anti-cancer drugs in a genome-wide manner (Behan et al., 2019; Huang et al., 2020; Tzelepis et al., 2016).

The current study aimed to clarify the underlying mechanisms for the conversion of curcumin β-D-glucuronide into aglycone curcumin in vivo as well as its antitumor effects. We also aimed to identify the essential therapeutic targets for antitumor effects of aglycone curcumin using genome-wide CRISPR-Cas9 screen. Since we have developed a synthetic curcumin β-D-glucuronide sodium salt (TBP1901), which is a higher water solubility and chemical stability than CMG, we decided to use TBP1901 for the current study and subsequent investigation.

2. Materials and Methods

2.1. Chemicals

Curcumin was purchased from FUJIFILM Wako Pure Chemical (Osaka, Japan), and bortezomib was obtained from AdooQ BioScience (CA, USA). Curcumin β-D-glucuronide sodium salt (TBP1901) was synthesized using the slightly modified method of a previous study (Ozawa et al., 2017). Chemical features of TBP1901 are summarized below.

^{1}H NMR (400 MHz, DMSO-d_6) δ 7.57 (d, J = 15.8 Hz, 1H), 7.55 (d, J = 15.8 Hz, 1H), 7.37 (d, J = 1.7 Hz, 1H), 7.32 (d, J = 1.7 Hz, 1H), 7.23 (dd, J = 8.6, 1.7 Hz, 1H), 7.14 (dd, J = 8.0, 1.7 Hz, 1H), 7.12 (d, J = 8.6 Hz, 1H), 6.84 (d, J = 15.8 Hz, 1H), 6.83 (d, J = 8.0 Hz, 1H), 6.76 (d, J = 15.8 Hz, 1H), 6.09 (s, 1H), 5.22 (brs, 1H), 5.03, (brs, 1H), 4.96 (d, J = 7.4 Hz, 1H), 3.85 (s, 3H), 3.83 (s, 3H), 3.43 (d, J = 9.5 Hz, 1H), 3.30–3.22 (m, 2H), 3.15 (dd, J = 9.5, 9.5 Hz, 1H). ^{13}C NMR (101 MHz, DMSO-d_6) δ 183.8, 182.5, 171.8, 149.6, 149.2, 148.7, 148.0, 141.0, 140.0, 128.6, 126.2, 123.2, 122.5, 121.1, 115.7, 115.3, 111.3, 111.2, 101.0, 99.7, 77.0, 73.6, 73.0, 72.0, 55.8, 55.7. HR-MS (ESI) m/z: [M-Na]$^-$ Calcd for $C_{27}H_{27}O_{12}^-$ 543.1508; found 543.1509. Melting point: 196 °C (decomp).

2.2. Measurement of curcumin β-D-glucuronide and aglycone curcumin levels in vivo

Five-week-old male C57BL/6J or C3H/HeJ mice (n = 6 per group, from CLEA Japan, Inc., Tokyo, Japan) received intravenous TBP1901 at a dose of 30 mg/kg. C3H/HeJ mice have a low GUSB activity due to the impaired GUSB gene (Gwynn et al., 1998). Saline solution was administered intravenously in C57BL/6J mice (n = 3) in the control group. Blood sample was collected 30 min after TBP1901 or saline solution administration. Another five-week-old male C57BL/6J mice (n = 5) received intravenous TBP1901 at a dose of 30 mg/kg. Thirty minutes after TBP1901 administration, blood, bone marrow, lung, heart, liver, kidney samples were collected, rapidly frozen in liquid nitrogen and stored at −80 °C. For the measurement of aglycone curcumin concentration in the bone marrow, 2.5% formic acid/methanol solution (for GUSB inhibition) and acetate buffer (pH 5.0) were added to the bone marrow and homogenized under ice-cold conditions followed by chloroform extraction. Curcumin β-D-glucuronide and aglycone curcumin levels were measured as previously reported (Ozawa et al., 2017).

2.3. Cynomolgus monkey experiment

Animal experiments using cynomolgus monkeys were conducted at Shin Nippon Biomedical Laboratories Ltd (Kagoshima, Japan). Two male and two female cynomolgus monkeys (4–5 years old) received 500 mg/kg of TBP1901 intravenously for 1 h. Blood and femurs samples were collected 30 min and 1–2 h after TBP1901 administration, respectively. Bone marrow fluid was harvested from the obtained femurs, which was rapidly frozen in liquid nitrogen and stored at −80 °C. Then, 2.5% formic acid/methanol solution (for GUSB inhibition) and acetate buffer (pH 5.0) were added to the bone marrow and homogenized under ice-cold conditions, followed by chloroform extraction to determine the aglycone curcumin concentration in the bone marrow. Curcumin β-D-glucuronide and aglycone curcumin were measured as previously reported (Ozawa et al., 2017). The conversion rate of TBP1901 to aglycone curcumin was calculated using the following formula: aglycone curcumin levels/[aglycone curcumin levels + curcumin β-D-glucuronide levels] × 100 (%).

2.4. GUSB activity assay

GUSB activity in tissues was measured using the Beta-Glucuronidase Activity Assay Kit (Abcam, Cambridge, UK) according to the instruction. Tumor-bearing mice with KMS11/BTZ cells were non-treated (control) or treated with TBP1901 at a dose of 30 mg/kg three times a week for two weeks. The tumors, bone marrow cells, and heart were extracted on day 14 GUSB and were frozen until use. The samples were processed according to the instructions and the fluorescence intensity (Ex/Em = 330/450 nm) was measured during incubation at 37 °C for 60 min. The activity was calculated per tissue weight.

2.5. Cell culture

KMS11 and bortezomib-resistant KMS11 (KMS/BTZ) (Ri et al., 2010) were purchased from JCRB Cell Bank (Osaka, Japan.). RPMI-1640 medium, FBS, and penicillin/streptomycin solution were purchased from Sigma Aldrich (St. Louis, MO, USA). AMO1 is a kind gift from Dr. Masaki Ri. All cells were cultured according to the following protocol: every three days in RPMI-1640 medium with 10% FBS and 1% penicillin/streptomycin solution at 37 °C in an atmosphere containing 5% CO2.

2.6. Genome-wide CRISPR-Cas9 screen

Cas9-expressing AMO1 cells were selected by Blasticidin at 10 μg/mL two days after lentiviral transduction using pKLV2-EF1aBsd2ACas9-W (Addgene #68343). Cas9 activity was confirmed using a lentiviral reporter pKLV2-U6gRNA(gGFP)-PGKBFP2AGFP-W (Addgene #67980). A total of 2.4 × 10^8 cells was transduced with the lentiviral-packaged Human v3 Genome-wide Knockout CRISPR Library at MOI 0.3 (Ong et al., 2017). Transduction efficiency was assessed three days after transduction and samples that showed 25–35% blue fluorescent protein (BFP)-positive were selected with puromycin at 4.0 μg/mL for four days

and further cultured. Nine days after transduction, 7.5×10^7 cells were collected for control and 5.0×10^7 cells were treated with DMSO at 0.1% or curcumin at 16.0 μM. Cells were maintained for 15 days with a minimum of 5.0×10^7 cells reseeded at each passage. Genomic DNA extraction and PCR amplification were performed as previously reported (Tzelepis et al., 2016). DNBSEQ-G400 was used for sequencing. Guide RNA count data were analyzed using Model-based Analysis of Genome-wide CRISPR/Cas9 Knockout (MAGeCK) statistical package (Li et al., 2014) by comparing curcumin-treated and DMSO-treated cells or by independently comparing curcumin or DMSO-treated cells with pre-treated cells as a control. The X–Y plots were depicted with gene-level log-fold change (LFC) computed with the latter.

Statistical enrichment of pathways in the ranked gene list from the gene-level LFC (Curcumin vs DMSO comparison) was carried out with Gene-set enrichment analysis (GSEA: Version 4.2.1) (Mootha et al., 2003; Subramanian et al., 2005), using gene sets from the Molecular Signature Database (MSigDB) (Mootha et al., 2003; Subramanian et al., 2005).

2.7. Assessment of the efficacy of TBP1901 in a bortezomib-resistant MM xenograft mice model

All experiments of mice were approved by the Institutional Animal Care and Use Committee of Jikei University (Permission No. 2018-004C1). The KMS11/BTZ cells (1×10^7) were subcutaneously transplanted in 6-week-old female NOD.CB17-Prkdcscid/J mice (n = 6 per group, Charles River Laboratories Japan, Inc., Tokyo, Japan). They were grouped 14 days after transplantation via a stratified randomization according to tumor volume. TBP1901 was administered intraperitoneally at a dose of 30 or 90 mg/kg three times a week for three weeks. According to a previously published report (Muraoka et al., 2019), bortezomib was administered intraperitoneally twice a week at a dose of 1 mg/kg for three weeks. Tumor volume was calculated as length × $\text{width}^2 \times 0.5$ (mm^3) on days 0, 7, 14, and 21 using a pair of calipers. Body weight was measured on days 0, 7, 14, and 21 using electronic scales (UW42005, Shimadzu, Kyoto, Japan).

2.8. Cell proliferation assay

KMS11 and KMS11/BTZ cells were plated in 96-well plates at 5×10^3 cells per well. The cells were subsequently treated after 24 h with TBP1901, aglycone curcumin or bortezomib at an indicated concentration for 72 h. Then, the cell viability was analyzed with the 3-(4,5-dimethylthiazol-2-yl)-5-(3- carboxymethoxyphenyl)-2-(4-sulfophenyl)-2H-tetrazolium, inner salt) (MTS) assay using the CellTiter 96 AQueous One Solution Cell Proliferation Assay (Promega Corporation, WI, USA).

2.9. NF-κB activity assay

KMS11 and KMS11/BTZ cells were plated in 96-well plates at 2×10^4 cells per well, and cultured in RPMI-1640 medium (1% FBS) for 24 h. These cells were transfected with pGL4.32 luc2P/NF-κB-RE plasmid (Promega) and pSF-PromMCS-βGal containing CMV promoters (Boca Scientific, MA, USA) using Lipofectamine 2000 Transfection Reagent (Invitrogen, CA, USA). After 3 h, transfected cells were treated with aglycone curcumin at an indicated concentration in RPMI-1640 medium (1% FBS) for 3 h. Then, the NF-κB activity was measured using Bright-Glo™ Luciferase Assay (Promega). The β-galactosidase activity was measured using β-Galactosidase Assay Kit (OZ Biosciences, CA, USA). NF-κB activity was shown as luciferase/β-galactosidase.

2.10. In vitro kinase assay

Recombinant GST-tagged kinases and their substrates were obtained from SignalChem (FL. USA). Protein kinase assays were performed using ADP-Glo™ Assay Kit (Promega). The assay conditions (enzyme and substrate amounts) were optimized to yield an acceptable enzymatic activity and high signal-to-noise ratios as detected using the instrument (GloMax, Promega). Reactions were performed for 40 min at room temperature in a 384-well plate and at a final well ATP concentration of 25 μM. Half maximal inhibitory concentration (IC_{50}) analysis was conducted using GraphPad Prism® version 5.01 (GraphPad Software, San Diego, CA, USA).

2.11. Chymotrypsin-like proteasome activity assay

KMS11 and KMS11/BTZ cells were plated in 96-well plates (concentration: 1×10^4 cells per well). Plated cells were treated after 24 h with aglycone curcumin or bortezomib at an indicated concentration for one or 3 h. The chymotrypsin-like proteasome activity was measured using Cell-Based Proteasome-Glo™ Assay (Promega).

2.12. Measurement of reactive oxygen species

KMS11 cells were plated in 96-well plates at 2×10^4 cells per well. After 24 h, the cells were treated with curcumin at an indicated concentration for 2 h. The levels of hydrogen peroxide (H_2O_2) in the cells were measured using ROS-Glo™ H_2O_2 Assay (Promega).

2.13. Reactive oxygen species inhibition assay

KMS11 cells were plated in 96-well plates at 5×10^3 cells per well. After 24 h, the cells were pretreated with an indicated concentration of *N*-acetyl-L-cysteine (NAC) (Merck KGaA, Darmstadt, Germany) for 24 h, then the cells were treated with curcumin and NAC at an indicated concentration for 72 h. The levels of H_2O_2 in the cells were measured using ROS-Glo™ H2O2 Assay, and the cell viability was analyzed using MTS assay.

2.14. Immunohistochemistry

Tumor-bearing mice with KMS11/BTZ cells were treated with TBP1901 at a dose of 30 mg/kg three times a week for two weeks. The tumor tissues were extracted on day 14. The samples were then fixed with formalin and embedded in paraffin. After heat-induced antigen-retrieval at 95 °C for 20 min, sections were incubated overnight at 4 °C with rabbit monoclonal anti-human p65 antibody (1:600 dilution, Abcam). Images were captured with NanoZoomer Digital Pathology 2 (Hamamatsu, Shizuoka, Japan).

2.15. Statistical analysis

Data were shown as mean ± standard deviation (SD) in an in vitro study and mean ± standard error (SE) in an in vivo study. Differences were analyzed using the Student's t-test.

2.16. Ethical considerations

All animal experiments were approved by the Institutional Animal Care and Use Committee of Jikei University (Permission No. 2018-004C1).

3. Results

3.1. GUSB is responsible for the conversion of TBP1901 into aglycone curcumin in vivo

Chemical formulas of curcumin (aglycone curcumin), CMG (curcumin β-D-glucuronide), and TBP1901 (curcumin β-D-glucuronide sodium salt) are shown in Fig. 1A. Since GUSB is reported to hydrolyze

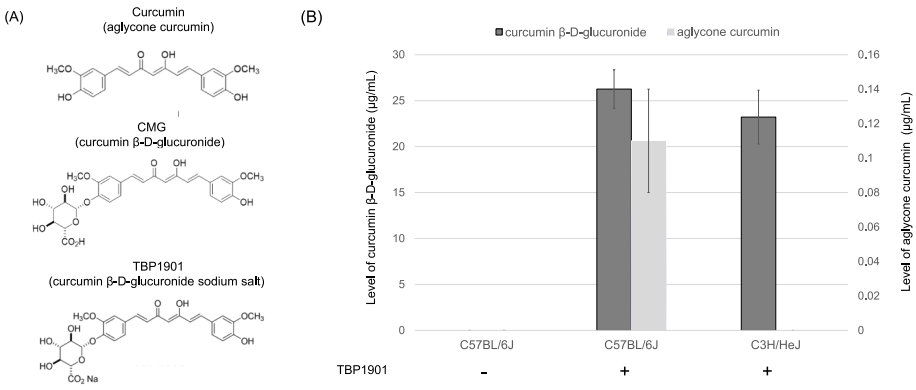

Fig. 1. Plasma curcumin β-D-glucuronide and aglycone curcumin levels after the intravenous administration of TBP1901 in GUSB-proficient or -impaired mice
(A) Chemical formula of curcumin β-D-glucuronide sodium salt (TBP1901) and aglycone curcumin (B) Plasma curcumin β-D-glucuronide and aglycone curcumin levels were evaluated 30 min after the intravenous administration of TBP1901 (30 mg/kg) in C57BL/6J (n = 5) or C3H/HeJ (n = 5) mice. As a control, plasma curcumin β-D-glucuronide and aglycone curcumin levels were assessed 30 min after intravenous administration of saline in C57BL/6J (n = 3). Data were presented as means ± SE.

glucuronide prodrugs (Sperker et al., 1997; Tranoy-Opalinski et al., 2014), we evaluated whether GUSB was responsible for the conversion of TBP1901 into curcumin using GUSB-proficient (C57BL/6J) and -impaired (C3H/HeJ) mice. Both curcumin β-D-glucuronide and aglycone curcumin were elevated in the plasma 30 min after TBP1901 injection in GUSB-proficient mice. However, only curcumin β-D-glucuronide, not aglycone curcumin, was elevated in GUSB-impaired mice (Fig. 1B). These results support the idea that GUSB is a key enzyme in converting TBP1901 to curcumin in vivo.

3.2. Conversion rate of TBP1901 to curcumin is highest in the bone marrow

The conversion rate of curcumin β-D-glucuronide to aglycone curcumin in major organs including the bone marrow, lung, heart, liver, and kidney, was tested in GUSB-proficient mice. The bone marrow had the highest aglycone curcumin levels 30 min after the single administration of TBP1901 at a dose of 30 mg/kg (Fig. 2A). The conversion rates of TBP1901 into aglycone curcumin were 0.3 (blood), 16.7 (bone marrow), 3.9 (lung), 8.8 (heart), 10.0 (liver), and 4.9 (kidney). The higher conversion rate of TBP1901 into curcumin in the bone marrow was then validated using cynomolgus monkeys. The curcumin β-D-glucuronide levels in the bone marrow and blood were 185 μg/g and 1919 μg/mL, respectively and the aglycone levels were 5.4 μg/g and 2.3 μg/mL in the bone marrow and plasma, respectively (Fig. 2B). In line with the results of the mice model, conversion rates of TBP1901 into curcumin in the bone marrow and plasma were 2.8 and 0.12, respectively.

3.3. GUSB activity is higher in bone marrow

Next, we measured GUSB activity in bone marrow. As expected higher GUSB activity was observed in bone marrow, which was line with the previous study reporting higher GUSB activity in bone marrow compared to heart, muscle and kidney in mice (Kunihiro et al., 2019). In tumor tissues, high GUSB activity was observed.

3.4. TBP1901 exhibits significant antitumor effects on bortezomib-resistant MM cells in vivo

To exploit the higher conversion rate of TBP1901 in the bone marrow, we considered that bone marrow cancer such as multiple myeloma (MM) could be a promising target disease of TBP1901 and tested its efficacy using MM cells in vitro and in vivo. In our previous study, TBP1901 demonstrated significant antitumor effects on oxaliplatin-resistant colon cancer cells in vivo (Ozawa-Umeta et al., 2020). In this study, efficacy of TBP1901 was tested in a xenograft model derived from bortezomib-resistant MM cells (KMS11/BTZ). As shown in Fig. 4A, the mean tumor volume of the control group increased over time

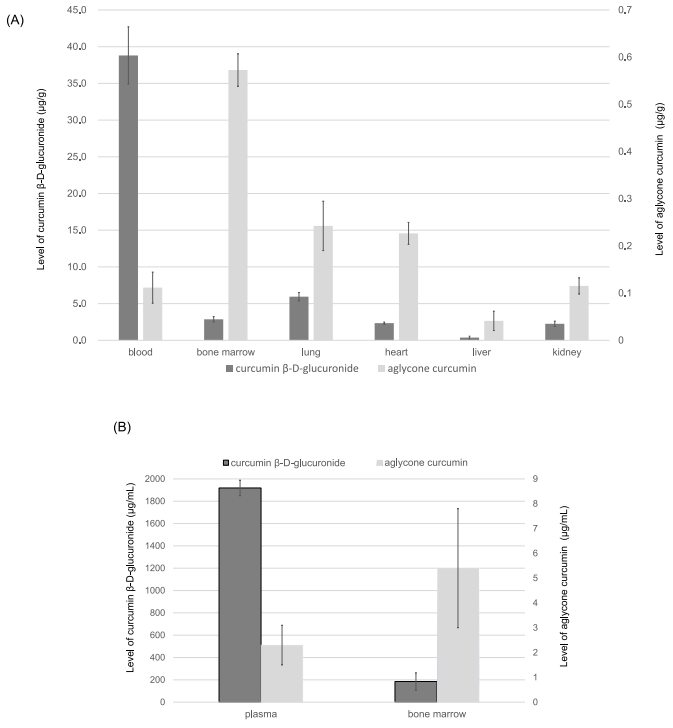

Fig. 2. Curcumin β-D-glucuronide and aglycone curcumin levels in the plasma and major organs after the intravenous administration of TBP1901
(A) Curcumin β-D-glucuronide and aglycone curcumin levels at indicated organs were measured 30 min after the intravenous administration of TBP1901 (30 mg/kg) in C57BL/6J (n = 5). Data were presented as means ± SE. (B) Plasma and bone marrow curcumin β-D-glucuronide and aglycone curcumin levels were evaluated after the intravenous administration of TBP1901 (500 mg/kg) in cynomolgus monkeys (n = 4). Data were presented as means ± SE.

from 70.0 ± 11.5 mm^3 on day 0–106.0 ± 16.8 mm^3 on day 21. The mean tumor volumes on day 21 were 97.4 ± 10.4 mm^3 in the bortezomib group, 61.3 ± 7.8 mm^3 in the 30 mg/kg TBP1901 group, and 44.8 ± 6.1 mm^3 in the 90 mg/kg TBP1901 group. Neither TBP1901 nor bortezomib showed a negative impact on body weight (Fig. 4B). Thus, TBP1901 significantly decreased tumor volume in a dose-dependent manner on bortezomib-resistant MM without causing weight loss.

3.5. TBP1901 has minimal effects on cell proliferation in vitro

To test the possibility that TBP1901 itself was involved in its antitumor effects in vivo, we examined its effects on cell proliferation using a pair of MM cell lines, KMS11 and KMS/BTZ, in vitro. In both cell lines, TBP1901 had minimal effects on cell proliferation even at a dose of 40

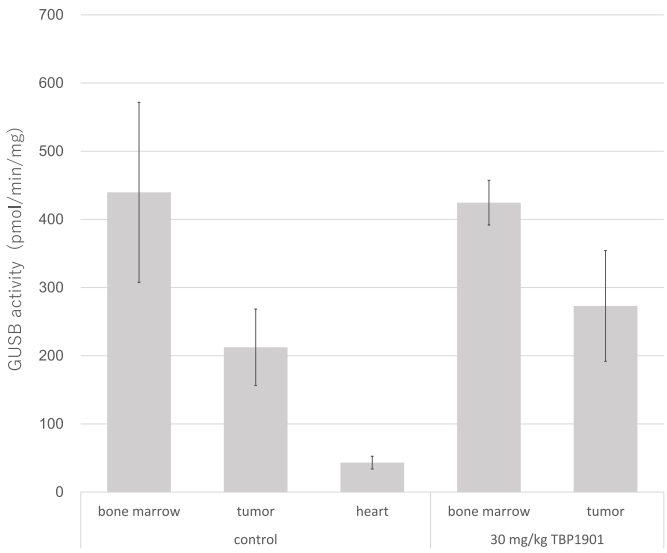

Fig. 3. GUSB activity in bone marrow, tumor, heart in control and TPB1901 treated mice.
Tumor-bearing mice with KMS11/BTZ cells were non-treated (control) or treated with TBP1901 at a dose of 30 mg/kg three times a week for two weeks. The indicated tissues were extracted on day 14 and GUSB activity were measured. Data were presented as means ± SE (n = 3, each).

μM, whereas its active metabolite, aglycone curcumin, suppressed cell proliferation in a dose-dependent manner (Fig. 5A and B). The IC_{50} values of aglycone curcumin were 22.2 and 13.3 μM for KMS11 and KMS11/BTZ, respectively.

3.6. *NF-κB signaling pathway and mitochondria related genes are among the highest hit by genome-wide CRISPR-Cas9 screen*

Agylcone curcumin is known to modulate multiple biological targets including NF-κB, proteasome, or ROS (Banerjee et al., 2019; Bharti et al., 2003; Kunnumakkara et al., 2007; Larasati et al., 2018; Milacic et al., 2008; Mizumoto et al., 2019). To prioritize therapeutic targets of aglycone curcumin among these multiple targets, we used a genome-wide CRISPR-Cas9 screen in this study. We investigated sgRNAs that were depleted or enriched in aglycone curcumin-treated cells by comparing the log fold change (LFC) of aglycone curcumin-treated cells with those treated with DMSO (Fig. 6A). Among the known therapeutic targets of aglycone curcumin, *NFKBIA* and *NFKBIB* were more depleted in aglycone curcumin-treated cells than in DMSO-treated cells, supporting the idea that NF-κB signaling pathway is involved in antitumor effects of aglycone curcumin (Fig. 6A). Next, we performed a pathway analysis with GSEA and found that a set of mitochondria-related genes (GO:0140053) was significantly enriched in aglycone curcumin treated cells (Fig. 6B), indicating that some mitochondrial function is required for aglycone curcumin induced antitumor effects. In contrast, proteasome-related gene sets were not significantly enriched or depleted in this screen (Fig. 6C).

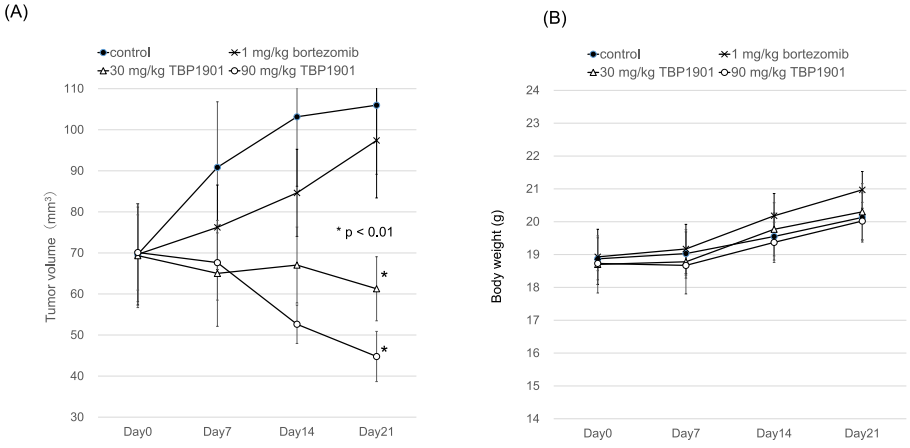

Fig. 4. Efficacy of TBP1901 against multiple myeloma cells in vivo and in vitro
(A) Tumor-bearing mice with KMS11/BTZ cells were treated with TBP1901 or bortezomib. TBP1901 was administered intraperitoneally at a dose of 30 or 90 mg/kg three times a week for three weeks and bortezomib was administered intraperitoneally twice a week at a dose of 1 mg/kg for three weeks. Tumor volume (left) and body weight (right) were presented as means ± SE (n = 6). *p < 0.01; as compared with the control group on day 21.

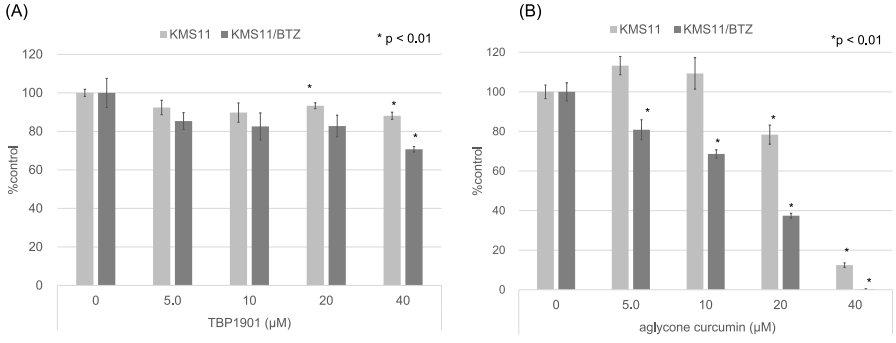

Fig. 5. Efficacy of TBP1901 against multiple myeloma cells in vitro
Effects of TBP1901 on the cell proliferation of KMS11 and KMS11/BTZ in vitro. Cells were treated with TBP1901 (A) or aglycone curcumin (B) at indicated concentrations for 72 h. Then, cell viability was evaluated by MTS assay. Data were presented as means ± SD. *p < 0.001, as compared with the control group.

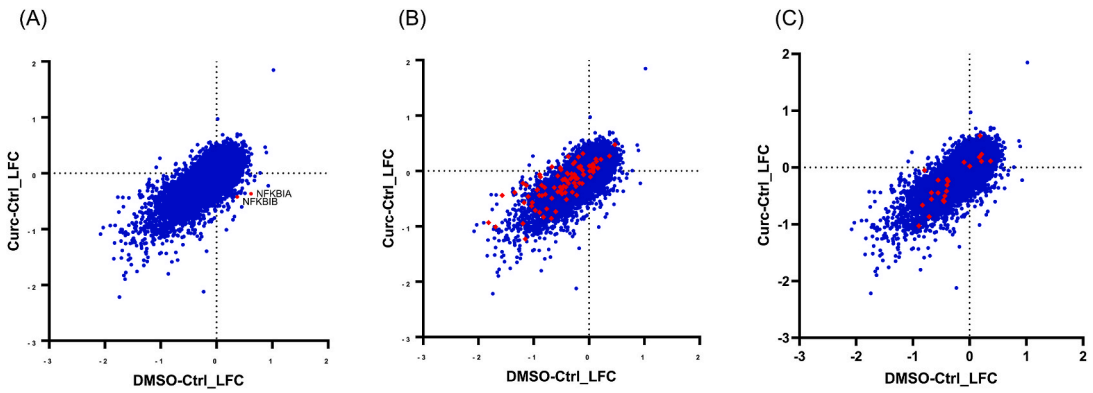

Fig. 6. Identification of the NF-κB signaling pathway and mitochondria-related genes by genome-wide CRISPR-Cas9 screen
(A, B, C) X–Y plot of gene-level log fold-change (LFC) of DMSO (X axis) versus curcumin (Y axis). *NFKBIA* and *NFKBIB* genes (A), mitochondria-related genes (n = 90, B), and proteasome-related genes (n = 22, C) are shown as red dots, whereas others are shown in blue dots.

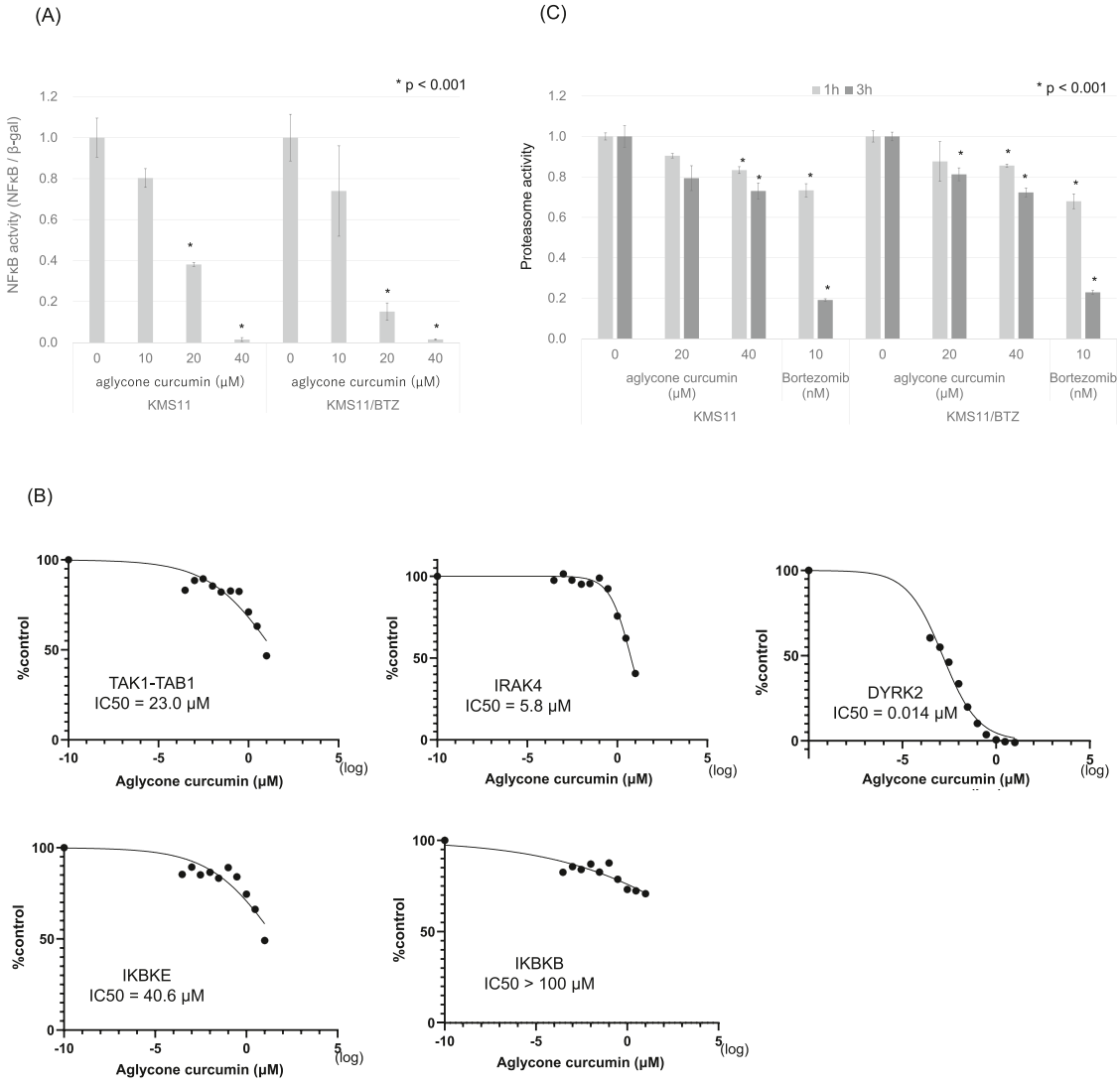

Fig. 7. Direct inhibition of protein kinases involved in the NF-κB signaling pathway by curcumin
(A) Dose-dependent inhibition of NF-κB activity by curcumin in KMS11 and KMS11/BTZ cells. Data were presented as means ± SD. *p < 0.001, as compared with the control group. (B) The protein kinase assays were performed as described in the Materials and Methods section. The IC_{50} graph was plotted using GraphPad Prism software. (C) Dose-dependent inhibition of chymotrypsin-like proteasome activity by curcumin in KMS11 and KMS11/BTZ cells. Data were presented as means ± SD. *p < 0.001, as compared with the control group.

3.7. Aglycone curcumin inhibits multiple protein kinases involved in NF-κB signaling pathway

To verify the results of the genome-wide CRISPR-Cas9 screen, we evaluated the effects of aglycone curcumin on the NF-κB signaling pathway in vitro. Significant inhibition of NF-κB activity by aglycone curcumin was validated in both KMS11 and KMS11/BTZ cell lines using a luciferase assay (Fig. 7A). The in vitro kinase assay was performed to validate the direct effects of aglycone curcumin on protein kinases involved in the NF-κB signaling pathway, including Interleukin 1 receptor associated kinase 4 (IRAK4), transforming growth factor β-activated kinase 1 (TAK1)/TAK1-binding protein 1 (TAB1), an inhibitor of nuclear factor-κB kinase subunit epsilon (IKBKE), and an inhibitor of nuclear factor-κB kinase subunit β (IKBKB), all of which were previously reported to be direct targets of curcumin (Bharti et al., 2003; Hsu et al., 2012; Li et al., 2019; Zhang et al., 2018). In addition, effects of aglycone curcumin on dual-specificity tyrosine-regulated kinase 2 (DYRK2), which is one of the known biological targets of curcumin (Banerjee et al., 2019) and could indirectly inhibit NF-κB activation through proteasome inhibition, were investigated. As shown in Fig. 7B, aglycone curcumin suppressed IRAK4 (IC_{50} = 5.8 μM), TAK1-TAB1 (IC_{50} = 23.0 μM), and DYRK2 (IC_{50} = 0.014 μM) within the comparable or lower dose required for cell growth inhibition in vitro. In contrast, aglycone curcumin exhibited modest inhibition against IKBKE (IC_{50} = 40.6 μM) and no potent inhibition on IKBKB (IC_{50} > 100 μM) in our current study.

Inhibitory effects of aglycone curcumin on chymotrypsin-like proteasome were also tested and curcumin inhibited proteasome activity by 20% and 30% at a dose of 20 μM and 40 μM, respectively (Fig. 7C).

3.8. Aglycone curcumin upregulates ROS induction

Since mitochondria respiration gene set was among the highest hit by CRISPR-Cas9 screen, and mitochondria is known to be a major source of cellular ROS, we tested the effects of aglycone curcumin on ROS induction in vitro. Aglycone curcumin induced ROS in a dose-dependent manner (Fig. 8A) and pretreatment of NAC completely inhibited ROS

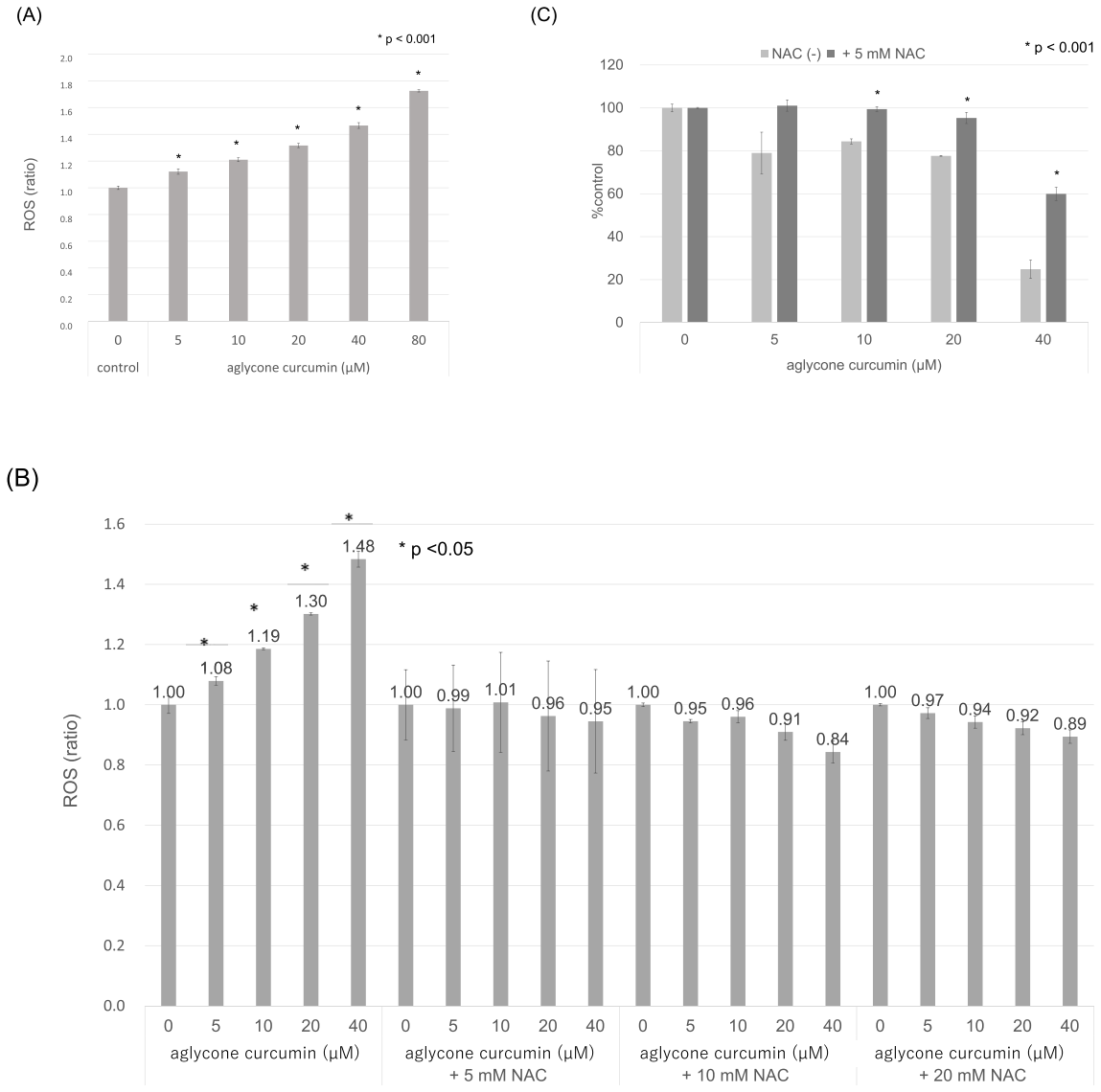

Fig. 8. ROS induction by curcumin and partial inhibition of antitumor effects of curcumin by ROS scavenger
(A) Dose-dependent induction of ROS by curcumin in KMS11. Data were presented as means ± SD. *p < 0.001; as compared with the control group. (B) KMS11 cells were pretreated with ROS scavenger, *N*-acetyl-L-cysteine (NAC), at indicated concentrations for 24 h and ROS induction was measured at indicated concentrations of aglycone curcumin. Data were presented as means ± SD. (C) Effects of NAC on cell proliferation of KMS11 under curcumin stimulation. Data were presented as means ± SD. *p < 0.001; as compared with the control group.

induction by aglycone curcumin (Fig. 8B) and partially reversed its antitumor effects in vitro (Fig. 8C).

4. Discussion

In this study, we demonstrated that GUSB is a pivotal enzyme in converting TBP1901 into aglycone curcumin in vivo. Our current results were in line with a previous study by Kunihiro et al., which reported that GUSB is a key enzyme in the metabolism of curcumin-glucuronide to aglycone curcumin in mice model (Kunihiro et al., 2019). GUSB is widely distributed in normal organs, but it is normally retained in the endoplasmic reticulum, while it is secreted extracellularly by monocytes/granulocytes in tumor or inflammatory tissues (Bosslet et al., 1998). High GUSB activity in the bone marrow as well as in tumor tissues were validated in our study (Fig. 3). Both aglylcone curcumin levels and conversion rate of TBP1901 into curcumin were highest in the bone marrow (Fig. 2A and B). Conversion rate of TBP1901 into curcumin was 50 times higher in the bone marrow than that in the blood. To exploit the higher conversion rate of TBP1901 in the bone marrow, we considered bone marrow cancer such as MM is a promising target disease for its clinical application and tested its efficacy on MM. It is ideal to test the efficacy of TBP1901 in orthotopic models; however, orthotopic mice models are not commonly used in the field of MM research. Moreover, tumor size change cannot be evaluated in orthotopic models during the treatment course. For these reasons, we selected a xenograft model in this study. On a bortezomib-resistant MM xenograft model, TBP1901 at a dose of 30 mg/kg showed significant antitumor effects. Of note, antitumor effects of TBP1901 was not limited to growth inhibition but induced tumor shrinkage. In previous studies demonstrating the efficacy of bortezomib on MM xenograft models, 1 mg/kg of bortezomib was reported to be effective in slowing tumor growth rate; however, bortezomib monotherapy did not demonstrate tumor shrinkage effects in any previous studies (LeBlanc et al., 2002; Muraoka et al., 2019; Sung et al., 2009). In addition, the gap between safety and efficacy was narrow in bortezomib. According to the animal toxicology data shown in the Food and Drug Administration package of bortezomib, monkeys died from cardiac toxicity after administration of twice the recommended clinical dose, which was converted to be approximately 0.2 mg/kg in nonrodent animals. Thus, the maximum tolerated dose (MTD) of bortezomib in monkeys was lower than the efficacy dose in mice. In contrast, in our toxicology study using cynomolgus monkeys, MTD of TBP1901 was determined to be 250 mg/kg (unpublished data). Since TBP1901 could exhibit antitumor effects at a dose of 30 mg/kg in mice model, MTD in monkeys is more than eight times higher than the efficacy dose in mice, indicating that this has a considerable safety margin. TBP1901's antitumor effects in vivo were unlikely to be derived from TBP1901 itself, since its effects on MM cell growth were negligible in vitro. Taken together, it is reasonable to assume that TBP1901 exerts its antitumor effects as a prodrug of aglycone curcumin in vivo.

Since aglycone curcumin can modulate multiple cancer-related biological pathways (Prasad et al., 2014), we employed a genome-wide CRISPR-Cas9 screen to prioritize its essential therapeutic targets. CRISPR-Cas9 screen disclosed *NFKB1A/NFKB1B*, which encode NF-κB inhibitory proteins (IκB) (Baeuerle and Baltimore, 1988), were among the highest hit genes (False discovery rate was 4.95E-04 for *NFKB1A* and 5.56E-02 for *NFKB1B*, respectively). Since a number of preclinical studies have proven that aglycone curcumin can inhibit NF-κB signaling pathway (Bharti et al., 2003; Kunnumakkara et al., 2007; Ozawa-Umeta et al., 2020; Singh and Aggarwal, 1995), the current results strongly support the idea that NF-κB inhibition is involved in the antitumor effects of aglycone curcumin. Aglycone curcumin suppressed the NF-κB activity of MM cells by $>$ 60% at a dose of 20 μM (Fig. 7A), which was almost equivalent to the IC_{50} required for cell growth inhibition in vitro. At a dose of 40 μM, curcumin almost completely abolished the NF-κB activity (Fig. 8A). In the in vitro kinase assay, curcumin directly suppressed IRAK4 and TAK1-TAB1 (Fig. 8B), both of which are the core components of the NF-κB signaling pathway, at a dose equivalent or lower than that of the IC_{50} required for cell growth inhibition. Immunohistochemical analysis showed reduced number of NF-κB positive cells in tumor tissues treated with TBP1901 compared to controls (Supplementary Fig. 1). In contrast, proteasome-related gene sets were not significantly enriched or depleted in CRISPR-Cas9 screen. In line with the results of CRISPR-Cas9 screen, inhibitory effects of curcumin on proteasome activity were modest (Fig. 7C). Furthermore, since curcumin suppressed cell proliferation of bortezomib-resistant KMS/BTZ cells, whose growth was unaffected despite bortezomib-induced proteasome inhibition, the direct contribution of proteasome inhibition to antitumor effects appeared to be minimal at least in our models.

Mitochondria respiration gene set was among the highest hits in the CRISPR-Cas9 screen. Mitochondria are well-known to be a major source of cellular ROS (Radak et al., 2013) and several research groups proposed that antitumor effects of curcumin is mediated by ROS induction (Fang et al., 2005; Larasati et al., 2018; Mizumoto et al., 2019; Woo et al., 2003). We validated that aglycone curcumin could induce ROS in a dose dependent manner, whereas NAC partially reversed its antitumor effects in vitro (Fig. 8A and C). These results support the idea that antitumor effects of curcumin are partly attributable to ROS induction. However, our current experiments were not sufficient to verify the real targets of TBP1901 in vivo. Furthermore, since aglycone curcumin can modulate multiple cancer-related biological pathways, further studies are warranted. MM is the second most common hematologic malignancy worldwide (Kazandjian, 2016). Over the past few decades, bortezomib, a proteasome inhibitor, has been a key drug for the treatment of MM. With the recent approval of novel drugs such as next-generation proteasome inhibitors (carfilzomib and ixazomib), monoclonal antibodies (daratumumab, elotuzumab, and isatuximab), immunomodulatory agent (pomalidomide), and histone-deacetylase inhibitor (panobinostat), the survival of patients with MM has been prolonged (Attal et al., 2019; Dimopoulos et al., 2016, 2017, 2018; Richardson et al., 2019; San-Miguel et al., 2014). Several researchers tested the efficacy of oral aglycone curcumin in patients with MM, and a few anecdotal efficacy signs were reported (Golombick et al., 2012; Ramakrishna et al., 2020; Zaidi et al., 2017). Zaidi et al. reported a patient with MM who started oral aglycone curcumin at a dose of 8 g after the third relapse and remained stable without any other treatment for more than 5 years, with a good quality of life (Zaidi et al., 2017). However, considering the poor bioavailability of oral aglycone curcumin, such a case seemed to be exceptional. In addition, MM is a disease of the elderly and the median age at the time of diagnosis is approximately 70 years old (Moreau and Touzeau, 2015). Therefore, there is still a need for developing novel MM treatments with minimum toxicity.

5. Conclusions

TBP1901 exhibits significant antitumor effects as a prodrug of curcumin and GUSB plays a pivotal role of conversion of TBP1901 into curcumin. Although aglycone curcumin can modulate multiple cancer-related biological pathways, genome-wide CRISPR-Cas9 screen disclosed that essential therapeutic targets of aglycone curcumin constitute NF-κB signaling pathway and ROS induction. To exploit the higher conversion rate of TBP1901 in the bone marrow, its clinical application for bone marrow disease like multiple myeloma is warranted.

CRediT authorship contribution statement

Tomoyuki Abe: Conceptualization, Methodology, Formal analysis, Investigation, Writing – original draft. **Yoshihito Horisawa:** Formal analysis, Investigation. **Osamu Kikuchi:** Formal analysis, Writing – original draft. **Hitomi Ozawa-Umeta:** Investigation. **Atsuhiro Kishimoto:** Conceptualization, Methodology, Formal analysis, Investigation. **Yasuhiro Katsuura:** Conceptualization, Methodology, Formal analysis, Investigation. **Atsushi Imaizumi:** Conceptualization, Methodology,

Formal analysis, Investigation. **Tadashi Hashimoto:** Supervision. **Kotaro Shirakawa:** Formal analysis, Investigation. **Akifumi Takaori-Kondo:** Supervision, Funding acquisition. **Kosuke Yusa:** Formal analysis, Funding acquisition, Writing – review & editing. **Tadashi Asakura:** Resources. **Hideaki Kakeya:** Supervision, Funding acquisition, Writing – review & editing. **Masashi Kanai:** Conceptualization, Formal analysis, Writing – original draft.

Declaration of competing interest

The authors declare the following financial interests/personal relationships which may be considered as potential competing interests: Tadashi Hashimoto is the chief executive officer of Therabiopharma Inc. Atushi Imaizumi is the senior vice president of Therabiopharma Inc. Tomoyuki Abe, Hitomi Ozawa-Umeta, Atsuhiro Kishimoto, and Yasuhiro Katsuura are employees of Therabiopharma Inc. Masashi Kanai. and Hideaki Kakeya own equity and they are the scientific consultants of Therabiopharma Inc.

Data availability

Data will be made available on request.

Acknowledgments

We thank Mr. S. Watari (Kyoto University) for measurement of HR-MS (ESI) of TBP1901. This work was supported in part by a Grant-in Aid for Scientific Research on Innovative Areas “Frontier Research on Chemical Communications” (No. 17H06401 to H.K.), a Grant-in-Aid for Scientific Research (B) (No. JP19H03502 to A. T-K.) from the Ministry of Education, Culture, Sports, Science, and Technology (MEXT), Japan, and Takeda Science Foundation (to K.Y.).

Appendix A. Supplementary data

Supplementary data to this article can be found online at https://doi.org/10.1016/j.ejphar.2022.175321.

References

Antony, B., Merina, B., Iyer, V.S., Judy, N., Lennertz, K., Joyal, S., 2008. A pilot cross-over study to evaluate human oral bioavailability of BCM-95CG (Biocurcumax), A novel Bioenhanced preparation of curcumin. Indian J. Pharmaceut. Sci. 70, 445–449.

Asher, G.N., Xie, Y., Moaddel, R., Sanghvi, M., Dossou, K.S., Kashuba, A.D., Sandler, R.S., Hawke, R.L., 2017. Randomized pharmacokinetic crossover study comparing 2 curcumin preparations in plasma and rectal tissue of healthy human volunteers. J. Clin. Pharmacol. 57, 185–193.

Attal, M., Richardson, P.G., Rajkumar, S.V., San-Miguel, J., Beksac, M., Spicka, I., Leleu, X., Schjesvold, F., Moreau, P., Dimopoulos, M.A., Huang, J.S., Minarik, J., Cavo, M., Prince, H.M., Mace, S., Corzo, K.P., Campana, F., Le-Guennec, S., Dubin, F., Anderson, K.C., group, I.-M.s., 2019. Isatuximab plus pomalidomide and low-dose dexamethasone versus pomalidomide and low-dose dexamethasone in patients with relapsed and refractory multiple myeloma (ICARIA-MM): a randomised, multicentre, open-label, phase 3 study. Lancet 394, 2096–2107.

Baeuerle, P.A., Baltimore, D., 1988. I kappa B: a specific inhibitor of the NF-kappa B transcription factor. Science 242, 540–546.

Banerjee, S., Wei, T., Wang, J., Lee, J.J., Gutierrez, H.L., Chapman, O., Wiley, S.E., Mayfield, J.E., Tandon, V., Juarez, E.F., Chavez, L., Liang, R., Sah, R.L., Costello, C., Mesirov, J.P., de la Vega, L., Cooper, K.L., Dixon, J.E., Xiao, J., Lei, X., 2019. Inhibition of dual-specificity tyrosine phosphorylation-regulated kinase 2 perturbs 26S proteasome-addicted neoplastic progression. Proc. Natl. Acad. Sci. U. S. A. 116, 24881–24891.

Behan, F.M., Iorio, F., Picco, G., Goncalves, E., Beaver, C.M., Migliardi, G., Santos, R., Rao, Y., Sassi, F., Pinnelli, M., Ansari, R., Harper, S., Jackson, D.A., McRae, R., Pooley, R., Wilkinson, P., van der Meer, D., Dow, D., Buser-Doepner, C., Bertotti, A., Trusolino, L., Stronach, E.A., Saez-Rodriguez, J., Yusa, K., Garnett, M.J., 2019. Prioritization of cancer therapeutic targets using CRISPR-Cas9 screens. Nature 568, 511–516.

Bharti, A.C., Donato, N., Singh, S., Aggarwal, B.B., 2003. Curcumin (diferuloylmethane) down-regulates the constitutive activation of nuclear factor-kappa B and IkappaBalpha kinase in human multiple myeloma cells, leading to suppression of proliferation and induction of apoptosis. Blood 101, 1053–1062.

Bosslet, K., Straub, R., Blumrich, M., Czech, J., Gerken, M., Sperker, B., Kroemer, H.K., Gesson, J.P., Koch, M., Monneret, C., 1998. Elucidation of the mechanism enabling tumor selective prodrug monotherapy. Cancer Res. 58, 1195–1201.

Dhillon, N., Aggarwal, B.B., Newman, R.A., Wolff, R.A., Kunnumakkara, A.B., Abbruzzese, J.L., Ng, C.S., Badmaev, V., Kurzrock, R., 2008. Phase II trial of curcumin in patients with advanced pancreatic cancer. Clin. Cancer Res. 14, 4491–4499.

Dimopoulos, M.A., Goldschmidt, H., Niesvizky, R., Joshua, D., Chng, W.J., Oriol, A., Orlowski, R.Z., Ludwig, H., Facon, T., Hajek, R., Weisel, K., Hungria, V., Minuk, L., Feng, S., Zahlten-Kumeli, A., Kimball, A.S., Moreau, P., 2017. Carfilzomib or bortezomib in relapsed or refractory multiple myeloma (ENDEAVOR): an interim overall survival analysis of an open-label, randomised, phase 3 trial. Lancet Oncol. 18, 1327–1337.

Dimopoulos, M.A., Lonial, S., Betts, K.A., Chen, C., Zichlin, M.L., Brun, A., Signorovitch, J.E., Makenbaeva, D., Mekan, S., Sy, O., Weisel, K., Richardson, P.G., 2018. Elotuzumab plus lenalidomide and dexamethasone in relapsed/refractory multiple myeloma: extended 4-year follow-up and analysis of relative progression-free survival from the randomized ELOQUENT-2 trial. Cancer 124, 4032–4043.

Dimopoulos, M.A., Oriol, A., Nahi, H., San-Miguel, J., Bahlis, N.J., Usmani, S.Z., Rabin, N., Orlowski, R.Z., Komarnicki, M., Suzuki, K., Plesner, T., Yoon, S.S., Ben Yehuda, D., Richardson, P.G., Goldschmidt, H., Reece, D., Lisby, S., Khokhar, N.Z., O’Rourke, L., Chiu, C., Qin, X., Guckert, M., Ahmadi, T., Moreau, P., Investigators, P., 2016. Daratumumab, lenalidomide, and dexamethasone for multiple myeloma. N. Engl. J. Med. 375, 1319–1331.

Fang, J., Lu, J., Holmgren, A., 2005. Thioredoxin reductase is irreversibly modified by curcumin: a novel molecular mechanism for its anticancer activity. J. Biol. Chem. 280, 25284–25290.

Golombick, T., Diamond, T.H., Manoharan, A., Ramakrishna, R., 2012. Monoclonal gammopathy of undetermined significance, smoldering multiple myeloma, and curcumin: a randomized, double-blind placebo-controlled cross-over 4g study and an open-label 8g extension study. Am. J. Hematol. 87, 455–460.

Greil, R., Greil-Ressler, S., Weiss, L., Schonlieb, C., Magnes, T., Radl, B., Bolger, G.T., Vcelar, B., Sordillo, P.P., 2018. A phase 1 dose-escalation study on the safety, tolerability and activity of liposomal curcumin (Lipocurc) in patients with locally advanced or metastatic cancer. Cancer Chemother. Pharmacol. 82, 695–706.

Gwynn, B., Lueders, K., Sands, M.S., Birkenmeier, E.H., 1998. Intracisternal A-particle element transposition into the murine beta-glucuronidase gene correlates with loss of enzyme activity: a new model for beta-glucuronidase deficiency in the C3H mouse. Mol. Cell Biol. 18, 6474–6481.

Hsu, S., Kim, M., Hernandez, L., Grajales, V., Noonan, A., Anver, M., Davidson, B., Annunziata, C.M., 2012. IKK-epsilon coordinates invasion and metastasis of ovarian cancer. Cancer Res. 72, 5494–5504.

Huang, A., Garraway, L.A., Ashworth, A., Weber, B., 2020. Synthetic lethality as an engine for cancer drug target discovery. Nat. Rev. Drug Discov. 19, 23–38.

Jager, R., Lowery, R.P., Calvanese, A.V., Joy, J.M., Purpura, M., Wilson, J.M., 2014. Comparative absorption of curcumin formulations. Nutr. J. 13, 11.

Kanai, M., Imaizumi, A., Otsuka, Y., Sasaki, H., Hashiguchi, M., Tsujiko, K., Matsumoto, S., Ishiguro, H., Chiba, T., 2012. Dose-escalation and pharmacokinetic study of nanoparticle curcumin, a potential anticancer agent with improved bioavailability, in healthy human volunteers. Cancer Chemother. Pharmacol. 69, 65–70.

Kanai, M., Otsuka, Y., Otsuka, K., Sato, M., Nishimura, T., Mori, Y., Kawaguchi, M., Hatano, E., Kodama, Y., Matsumoto, S., Murakami, Y., Imaizumi, A., Chiba, T., Nishihira, J., Shibata, H., 2013. A phase I study investigating the safety and pharmacokinetics of highly bioavailable curcumin (Theracurmin) in cancer patients. Cancer Chemother. Pharmacol. 71, 1521–1530.

Kanai, M., Yoshimura, K., Asada, M., Imaizumi, A., Suzuki, C., Matsumoto, S., Nishimura, T., Mori, Y., Masui, T., Kawaguchi, Y., Yanagihara, K., Yazumi, S., Chiba, T., Guha, S., Aggarwal, B.B., 2011. A phase I/II study of gemcitabine-based chemotherapy plus curcumin for patients with gemcitabine-resistant pancreatic cancer. Cancer Chemother. Pharmacol. 68, 157–164.

Kazandjian, D., 2016. Multiple myeloma epidemiology and survival: a unique malignancy. Semin. Oncol. 43, 676–681.

Kunihiro, A.G., Luis, P.B., Brickey, J.A., Frye, J.B., Chow, H.S., Schneider, C., Funk, J.L., 2019. Beta-glucuronidase catalyzes deconjugation and activation of curcumin-glucuronide in bone. J Nat Prod 82, 500–509.

Kunnumakkara, A.B., Guha, S., Krishnan, S., Diagaradjane, P., Gelovani, J., Aggarwal, B. B., 2007. Curcumin potentiates antitumor activity of gemcitabine in an orthotopic model of pancreatic cancer through suppression of proliferation, angiogenesis, and inhibition of nuclear factor-kappaB-regulated gene products. Cancer Res. 67, 3853–3861.

Larasati, Y.A., Yoneda-Kato, N., Nakamae, I., Yokoyama, T., Meiyanto, E., Kato, J.Y., 2018. Curcumin targets multiple enzymes involved in the ROS metabolic pathway to suppress tumor cell growth. Sci. Rep. 8, 2039.

LeBlanc, R., Catley, L.P., Hideshima, T., Lentzsch, S., Mitsiades, C.S., Mitsiades, N., Neuberg, D., Goloubeva, O., Pien, C.S., Adams, J., Gupta, D., Richardson, P.G., Munshi, N.C., Anderson, K.C., 2002. Proteasome inhibitor PS-341 inhibits human myeloma cell growth in vivo and prolongs survival in a murine model. Cancer Res. 62, 4996–5000.

Li, Q., Chen, Y., Zhang, D., Grossman, J., Li, L., Khurana, N., Jiang, H., Grierson, P.M., Herndon, J., DeNardo, D.G., Challen, G.A., Liu, J., Ruzinova, M.B., Fields, R.C., Lim, K.H., 2019. IRAK4 mediates colitis-induced tumorigenesis and chemoresistance in colorectal cancer. JCI Insight 4.

Li, W., Xu, H., Xiao, T., Cong, L., Love, M.I., Zhang, F., Irizarry, R.A., Liu, J.S., Brown, M., Liu, X.S., 2014. MAGeCK enables robust identification of essential genes from genome-scale CRISPR/Cas9 knockout screens. Genome Biol. 15, 554.

Marczylo, T.H., Verschoyle, R.D., Cooke, D.N., Morazzoni, P., Steward, W.P., Gescher, A. J., 2007. Comparison of systemic availability of curcumin with that of curcumin formulated with phosphatidylcholine. Cancer Chemother. Pharmacol. 60, 171–177.
Milacic, V., Banerjee, S., Landis-Piwowar, K.R., Sarkar, F.H., Majumdar, A.P., Dou, Q.P., 2008. Curcumin inhibits the proteasome activity in human colon cancer cells in vitro and in vivo. Cancer Res. 68, 7283–7292.
Mizumoto, A., Ohashi, S., Kamada, M., Saito, T., Nakai, Y., Baba, K., Hirohashi, K., Mitani, Y., Kikuchi, O., Matsubara, J., Yamada, A., Takahashi, T., Lee, H., Okuno, Y., Kanai, M., Muto, M., 2019. Combination treatment with highly bioavailable curcumin and NQO1 inhibitor exhibits potent antitumor effects on esophageal squamous cell carcinoma. J. Gastroenterol. 54, 687–698.
Mootha, V.K., Lindgren, C.M., Eriksson, K.F., Subramanian, A., Sihag, S., Lehar, J., Puigserver, P., Carlsson, E., Ridderstrale, M., Laurila, E., Houstis, N., Daly, M.J., Patterson, N., Mesirov, J.P., Golub, T.R., Tamayo, P., Spiegelman, B., Lander, E.S., Hirschhorn, J.N., Altshuler, D., Groop, L.C., 2003. PGC-1alpha-responsive genes involved in oxidative phosphorylation are coordinately downregulated in human diabetes. Nat. Genet. 34, 267–273.
Moreau, P., Touzeau, C., 2015. Multiple Myeloma: from Front-Line to Relapsed Therapies. Am Soc Clin Oncol Educ Book, pp. e504–e511.
Muraoka, H., Yoshimura, C., Kawabata, R., Tsuji, S., Hashimoto, A., Ochiiwa, H., Nakagawa, F., Fujioka, Y., Matsuo, K., Ohkubo, S., 2019. Activity of TAS4464, a novel NEDD8 activating enzyme E1 inhibitor, against multiple myeloma via inactivation of nuclear factor kappaB pathways. Cancer Sci. 110, 3802–3810.
Ong, S.H., Li, Y., Koike-Yusa, H., Yusa, K., 2017. Optimised metrics for CRISPR-KO screens with second-generation gRNA libraries. Sci. Rep. 7, 7384.
Ozawa-Umeta, H., Kishimoto, A., Imaizumi, A., Hashimoto, T., Asakura, T., Kakeya, H., Kanai, M., 2020. Curcumin beta-D-glucuronide exhibits anti-tumor effects on oxaliplatin-resistant colon cancer with less toxicity in vivo. Cancer Sci. 111, 1785–1793.
Ozawa, H., Imaizumi, A., Sumi, Y., Hashimoto, T., Kanai, M., Makino, Y., Tsuda, T., Takahashi, N., Kakeya, H., 2017. Curcumin beta-D-glucuronide plays an important role to keep high levels of free-form curcumin in the blood. Biol. Pharm. Bull. 40, 1515–1524.
Prasad, S., Gupta, S.C., Tyagi, A.K., Aggarwal, B.B., 2014. Curcumin, a component of golden spice: from bedside to bench and back. Biotechnol. Adv. 32, 1053–1064.
Radak, Z., Zhao, Z., Koltai, E., Ohno, H., Atalay, M., 2013. Oxygen consumption and usage during physical exercise: the balance between oxidative stress and ROS-dependent adaptive signaling. Antioxidants Redox Signal. 18, 1208–1246.
Ramakrishna, R., Diamond, T.H., Alexander, W., Manoharan, A., Golombick, T., 2020. Use of Curcumin in Multiple Myeloma patients intolerant of steroid therapy. Clin Case Rep 8, 739–744.
Ri, M., Iida, S., Nakashima, T., Miyazaki, H., Mori, F., Ito, A., Inagaki, A., Kusumoto, S., Ishida, T., Komatsu, H., Shiotsu, Y., Ueda, R., 2010. Bortezomib-resistant myeloma cell lines: a role for mutated PSMB5 in preventing the accumulation of unfolded proteins and fatal ER stress. Leukemia 24, 1506–1512.
Richardson, P.G., Oriol, A., Beksac, M., Liberati, A.M., Galli, M., Schjesvold, F., Lindsay, J., Weisel, K., White, D., Facon, T., San Miguel, J., Sunami, K., O'Gorman, P., Sonneveld, P., Robak, P., Semochkin, S., Schey, S., Yu, X., Doerr, T., Bensmaine, A., Biyukov, T., Peluso, T., Zaki, M., Anderson, K., Dimopoulos, M., investigators, O.t., 2019. Pomalidomide, bortezomib, and dexamethasone for patients with relapsed or refractory multiple myeloma previously treated with lenalidomide (OPTIMISMM): a randomised, open-label, phase 3 trial. Lancet Oncol. 20, 781–794.
San-Miguel, J.F., Hungria, V.T., Yoon, S.S., Beksac, M., Dimopoulos, M.A., Elghandour, A., Jedrzejczak, W.W., Gunther, A., Nakorn, T.N., Siritanaratkul, N., Corradini, P., Chuncharunee, S., Lee, J.J., Schlossman, R.L., Shelekhova, T., Yong, K., Tan, D., Numbenjapon, T., Cavenagh, J.D., Hou, J., LeBlanc, R., Nahi, H., Qiu, L., Salwender, H., Pulini, S., Moreau, P., Warzocha, K., White, D., Blade, J., Chen, W., de la Rubia, J., Gimsing, P., Lonial, S., Kaufman, J.L., Ocio, E.M., Veskovski, L., Sohn, S.K., Wang, M.C., Lee, J.H., Einsele, H., Sopala, M., Corrado, C., Bengoudifa, B.R., Binlich, F., Richardson, P.G., 2014. Panobinostat plus bortezomib and dexamethasone versus placebo plus bortezomib and dexamethasone in patients with relapsed or relapsed and refractory multiple myeloma: a multicentre, randomised, double-blind phase 3 trial. Lancet Oncol. 15, 1195–1206.
Singh, S., Aggarwal, B.B., 1995. Activation of transcription factor NF-kappa B is suppressed by curcumin (diferuloylmethane) [corrected]. J. Biol. Chem. 270, 24995–25000.
Sperker, B., Backman, J.T., Kroemer, H.K., 1997. The role of beta-glucuronidase in drug disposition and drug targeting in humans. Clin. Pharmacokinet. 33, 18–31.
Stohs, S.J., Chen, O., Ray, S.D., Ji, J., Bucci, L.R., Preuss, H.G., 2020. Highly bioavailable forms of curcumin and promising avenues for curcumin-based research and application: a review. Molecules 25.
Subramanian, A., Tamayo, P., Mootha, V.K., Mukherjee, S., Ebert, B.L., Gillette, M.A., Paulovich, A., Pomeroy, S.L., Golub, T.R., Lander, E.S., Mesirov, J.P., 2005. Gene set enrichment analysis: a knowledge-based approach for interpreting genome-wide expression profiles. Proc. Natl. Acad. Sci. U. S. A. 102, 15545–15550.
Sung, B., Kunnumakkara, A.B., Sethi, G., Anand, P., Guha, S., Aggarwal, B.B., 2009. Curcumin circumvents chemoresistance in vitro and potentiates the effect of thalidomide and bortezomib against human multiple myeloma in nude mice model. Mol. Cancer Therapeut. 8, 959–970.
Tranoy-Opalinski, I., Legigan, T., Barat, R., Clarhaut, J., Thomas, M., Renoux, B., Papot, S., 2014. beta-Glucuronidase-responsive prodrugs for selective cancer chemotherapy: an update. Eur. J. Med. Chem. 74, 302–313.
Tzelepis, K., Koike-Yusa, H., De Braekeleer, E., Li, Y., Metzakopian, E., Dovey, O.M., Mupo, A., Grinkevich, V., Li, M., Mazan, M., Gozdecka, M., Ohnishi, S., Cooper, J., Patel, M., McKerrell, T., Chen, B., Domingues, A.F., Gallipoli, P., Teichmann, S., Ponstingl, H., McDermott, U., Saez-Rodriguez, J., Huntly, B.J.P., Iorio, F., Pina, C., Vassiliou, G.S., Yusa, K., 2016. A CRISPR dropout screen identifies genetic vulnerabilities and therapeutic targets in acute myeloid leukemia. Cell Rep. 17, 1193–1205.
Woo, J.H., Kim, Y.H., Choi, Y.J., Kim, D.G., Lee, K.S., Bae, J.H., Min, D.S., Chang, J.S., Jeong, Y.J., Lee, Y.H., Park, J.W., Kwon, T.K., 2003. Molecular mechanisms of curcumin-induced cytotoxicity: induction of apoptosis through generation of reactive oxygen species, down-regulation of Bcl-XL and IAP, the release of cytochrome c and inhibition of Akt. Carcinogenesis 24, 1199–1208.
Zaidi, A., Lai, M., Cavenagh, J., 2017. Long-term stabilisation of myeloma with curcumin. BMJ Case Rep. 2017.
Zhang, Z.B., Luo, D.D., Xie, J.H., Xian, Y.F., Lai, Z.Q., Liu, Y.H., Liu, W.H., Chen, J.N., Lai, X.P., Lin, Z.X., Su, Z.R., 2018. Curcumin's metabolites, tetrahydrocurcumin and octahydrocurcumin, possess superior anti-inflammatory effects in vivo through suppression of TAK1-NF-kappaB pathway. Front. Pharmacol. 9, 1181.